SCVJ
Volume 4, Issue 2, 2023
DOI: http://doi.org/10.55989/KLYA6292
Science View Journal
ISSN (Online): 2734-2638

Efficiency of Polymer-silica Blends in the Microencapsulation of Yellow Fever Virus Vaccine

I. A. Onah[1,2], K. C. Ofokansi[3], D. C. Odimegwu[1], E. B. Onuigbo[1]

[1]Department of Pharmaceutical Microbiology and Biotechnology, Faculty of Pharmaceutical Sciences, University of Nigeria, Nsukka, Nigeria.
[2]Department of Microbiology, Faculty of Natural Sciences, Caritas University, Enugu, Nigeria.
[3]Department of Pharmaceutics, Faculty of Pharmaceutical Sciences, University of Nigeria, Nsukka, Nigeria.

Email: ifeomaonah0813@gmail.com

Abstract:
The currently available yellow fever vaccines are thermally unstable and involve huge costs during preservation and administration. Microencapsulation with thermally stable coating materials is considered as a means of protecting yellow fever vaccines from thermal degradation. Silica nanoparticles have thermal stabilizing abilities but do not possess film forming properties. It is proposed that polymer-silica blends might be a good coating material for microencapsulation. This study is aimed at investigating the compatibility and efficiency of blends of selected polymers with silicon obtained from rice husk ash (RHA) in microencapsulating yellow fever virus vaccine. The encapsulated yellow fever vaccine was characterised by FTIR and SEM-EDX spectroscopy, and the vaccine encapsulation efficiency was determined. FTIR spectra of the individual components and final encapsulated vaccine showed good chemical compatibility of all the ingredients. SEM studies of the products revealed uneven and rough surfaces with shrinkages. The vaccine encapsulation efficiency was 66.7%. Altogether, these results suggest that polymer-RHA silica blend can be used in microencapsulating yellow fever virus vaccine.

Keywords: Chitosan, polymers, rice husks ash, silica nanoparticles, sodium alginate, microencapsulation, yellow fever vaccine.

I. INTRODUCTION

Yellow fever virus infection is an acute, life-threatening haemorrhagic disease that is a significant health problem in sub-Saharan Africa and tropical South America (Bassey et al., 2022; Luria-Pe´rez et al., 2022). However, it is preventable through vaccination. The currently available yellow fever vaccine is thermally unstable and incurs a huge cost during storage for parenteral administration (Bassey et al., 2022). This thermal instability of yellow fever vaccine is a challenge that needs to be tackled, because yellow fever virus is still endemic in many countries. Although the cold chain technology is a means of ensuring the potency of this thermolabile vaccine product, research has shown the inefficiency of the cold chain system in various quarters (Bankole et al., 2010; Oli et al., 2017) thereby necessitating the need to make yellow fever vaccine thermally stable. The huge cost incurred during storage, in addition to the problems of needle safety and low compliance because of the fear of injection, is also a cause for concern, thus necessitating the development of an oral thermostable yellow fever vaccine. Microencapsulation with thermal stable coating materials is one means of protecting the thermolabile yellow fever vaccine from heat. Microencapsulation is also a good alternative when creating an orally administered vaccine as encapsulation will protect the yellow fever vaccine antigen from the degradative enzymes present in the gastrointestinal tract. Silica nanoparticles (SiO2 NPs) from rice husks ash have thermal and chemical stabilizing properties, strong biocompatibility, permeability, high mechanical strength, low toxicity and simple synthetic approach (Alhadhrami et al., 2022; Ribeiro et al., 2014; Hung et al., 2018; Witoon et al., 2008) thus can be employed in the microencapsulation of yellow fever vaccine. Research has also shown that silica (SiO2) confers abiotic and biotic stress tolerance in monocot plants (Rains et al., 2006; Epstein, 2001). Silica, however, does not have film forming properties; thus, it cannot be used alone as a wall material except in combination with a film forming polymer (Ribeiro et al., 2014; Zhang et al., 2013; Shang et al., 2002). The silica content of the polymer-silica blend must be optimized in order to simultaneously increase the tensile strength and impact resistance, without decreasing its flexural properties. A polymer-silica blend with a silica content of ca. 10 wt% is usually found to give the best film properties (Ribeiro et al., 2014; Zhang et al., 2013; Shang et al., 2002). The incorporation of SiO2 NPs in polymer films is also known to enhance the film mechanical properties and to reduce its thermal degradation at high temperature, also improving its insulation properties, and increasing the barrier properties to solvents and volatile products (Ribeiro et al., 2014; Ray and Okamoto, 2003). A blend of organic/inorganic materials combine the rigidity and high thermal stability of the inorganic material (SiO2 NPs) with the flexibility, ductility and processability of the organic polymers (Ribeiro et al., 2014). Microencapsulation with polymers alone often results in a product not suitable for oral administration as polymeric

SCVJ
Volume 4, Issue 2, 2023
DOI: http://doi.org/10.55989/KLYA6292
Science View Journal
ISSN (Online): 2734-2638

nanoparticles are structurally unstable and susceptible to hydrolysis in the harsh stomach environment (Kumari et al., 2010). Often times the encapsulated material in the polymer matrix would trickle out within few hours due to the degradation or diffusion of the polymer matrix (Kumari et al., 2010). Polymer-silica blend might be a good coating material for the microencapsulation of yellow fever vaccine. The aim of the study therefore was to evaluate the compatibility and efficiency of polymer-silica blend in the microencapsulation of yellow fever vaccine.

II. Materials and Methods

SYNTHESIS OF SIO2 NPS FROM RICE HUSKS ASH (RHA)

Raw rice husks were gotten from a rice mill factory in Adani (Uzo-uwani LGA of Enugu State, Nigeria). SiO2 NPs from RHA were produced following the method of Sankar et al. (2016). Briefly, raw rice husk (RH) was washed with tap water to remove contaminants, and dried at 60oC in forced air oven (ShelLab USA, Model No. SM05). The washed and dried RH was burnt in a furnace (SearchTech Instruments China, Model No. SXL) to produce RHA. In order to separate the metal ions in RHA, 1000 ml of HCl 1N was added to 100 g of RHA, and the mixture was agitated at room temperature for 2 h and left overnight. The acid-treated RHA was filtered, rinsed with distilled water and dried at 60°C in forced air oven. The acid-treated RHA was then placed in a porcelain cup and subjected to a calcination process in the furnace at 700 °C for 2 h.

POLYMERS

The polymers used were chitosan (Sigma-Aldrich, USA) and sodium alginate (Sigma-Aldrich, USA).

VACCINE

Stamaril® (Sanofi Pasteur, UK), a commercial brand of yellow fever vaccine, was used. The product is a live attenuated yellow fever virus vaccine made from a 17D-204 strain of the yellow fever virus, produced in pathogen-free chick embryos.

MICROENCAPSULATION OF YELLOW FEVER VIRUS VACCINE IN POLYMER-SILICA BLEND

The silica nanoparticles, sodium alginate, calcium chloride and chitosan powders were sterilized via dry heat sterilization at 100oC for 1h. Yellow fever vaccine (YFV-17D-204, Stamaril®) was microencapsulated within alginate solution utilising an ionotropic gelation technique described by Yeung et al. (2016). Briefly, 1 g of sodium alginate was dissolved in 99 ml of distilled water to create a 1% w/v sodium alginate solution. The sterile alginate solution (95 ml) was then combined with 5 ml of reconstituted yellow fever virus vaccine (YFV), and then agitated to evenly spread out the virus. The final product was then formed by injecting with a 21 G X 1½ inch (0.8 X 38 mm) needle aliquots of virus/alginate solution into 400 ml of 0.1 M calcium chloride solution. After 1 h of agitated gelation with a magnetic stirrer (M21, Superior Marienfeld, Germany) at the rate of 400 rpm, the resultant microcapsules were collected by gravity filtration utilizing a muslin cloth and funnel, washed with sterile deionized water, and then re-filtered.

The microcapsules prepared were double coated with the RHA SiO2 NPs dispersed in chitosan. Aqueous chitosan solution (0.4 % w/v) was made following the procedure provided by Zhou et al. (1998) with some modification. In brief, 0.4 g of chitosan was dissolved in 1 % glacial acetic acid (100 ml) and 0.4g of the RHASiO2 NPs was dispersed in it. The pH was adjusted to 5.0 – 5.1 with 1M NaOH. Subsequently, the freshly prepared alginate microcapsules were dipped into the chitosan/SiO2 NPs solution to provide secondary coating as cationic chitosan molecules are attracted electrostatically to the surfaces of anionic alginate microcapsules. After one hour of stirring with a magnetic stirrer (M21, Superior Marienfeld, Germany), the mixture was filtered through a funnel with muslin cloth, and sterile distilled water was used to rinse the microcapsules. Chitosan-coated alginate microcapsules were afterwards kept until further studies.

FOURIER TRANSFORM INFRARED (FTIR) SPECTROSCOPY

The FTIR spectrum of the SiO2 NPs, polymers, calcium chloride and yellow fever vaccine were recorded with the Fourier-transform infrared spectrometer-Cary 660 FTIR (MIR system)(Agilent Technologies, USA). Samples were combined with 250 mg of potassium bromide (KBr) to obtain pellets. Spectral scanning was carried out in the range of 600–4000 cm–1 while the Fourier-transform infrared spectroscopy of the formulated nanocapsules was carried out with Schmadzu 8400s spectrophotometer (Schmadzu, Japan). The sample wasalso combined with 250 mg of potassium bromide and spectral scanning carried out in 600–4000 cm–1 range.

SCANNING ELECTRON MICROSCOPY-ENERGY DISPERSIVE X-RAY SPECTROSCOPY (SEM-EDX)

The microstructure and chemical composition of the yellow fever virus microcapsules vaccine prepared were examined with a scanning electron microscope attached with energy dispersive X-Ray Spectroscopy (PhenomProX with EDX, Phenom World Thermo Fisher Scientific, Netherlands) in the magnification range of 500 to 4,000. The samples were placed on aluminium stubs and using an ion coater was coated with gold up to 20 nm thickness. Then the photomicrographs were taken at an accelerating voltage of 10kV. During the energy dispersive X-Ray Spectroscopy measurement, two spots were focused and the corresponding peaks recorded.

VACCINE ENTRAPMENT EFFICIENCY (VEE)

In order to determine the vaccine entrapment efficiency, accurately weighed amounts (10 mg) of the microcapsule vaccine were grinded and mixed with 1 ml of distilled water. The mixture was centrifuged for five minutes at 3000 revolution per minute. The supernatant discarded and the

SCVJ
Volume 4, Issue 2, 2023
DOI: http://doi.org/10.55989/KLYA6292
Science View Journal
ISSN (Online): 2734-2638

sediment used to determine the viral load via hemagglutination assay (Grimes, 2002). A micropipette was used to remove 50 µl of the formulation sediments and dispensed into a well of the microtitre plate. Fifty µl of the commercial vaccine was placed in another well. Then 50 µl of properly washed 1 % dispersion of red blood cells was added to each well. This was mixed and a double fold serial dilution was carried out up to the last well on the row. A separate well containing only the 1 % red blood cells served as the negative control. This was left to stand for 30 minutes at room temperature, after which the results were recorded and the vaccine entrapment efficiency (VEE %) was calculated as follows:

$$\text{VEE } \% = \frac{t_1 - t_2}{t_1} \times 100 \qquad (1)$$

were t1 = number of wells in a roll
t2= number of wells in a row without haemaglutination

III. RESULTS

The synthesized rice husks ash SiO2 NPs was white in colour as shown in Figure 1. The FT-IR spectra of the RHA SiO2 NPs, polymers (sodium alginate and chitosan), calcium chloride, yellow fever virus vaccine and the newly formulated Polymer - Rice Silica –Yellow fever virus vaccine (PRSYFV) are presented in Figures 2-7. The texture of the PRSYFV microcapsule vaccine as recorded with the scanning electron microscope at an acceleration voltage of 10kV is shown in Figure 8. The microcapsules surface composition and crystal depositions as identified via EDX measurements are shown in Figure 9. The vaccine encapsulation efficiency recorded was 66.7%

Figure 1: Digital photograph of SiO2 NPs from Rice Husks Ash (RHA).

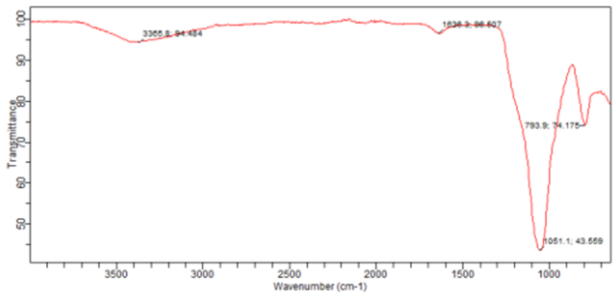

Figure 2: FT-IR spectrum of RHA SiO2 NPs.

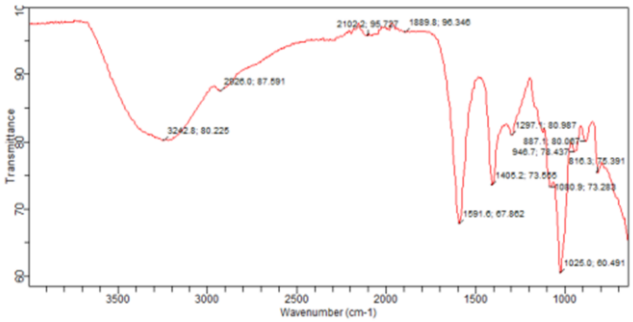

Figure 3: FT-IR spectrum of sodium alginate

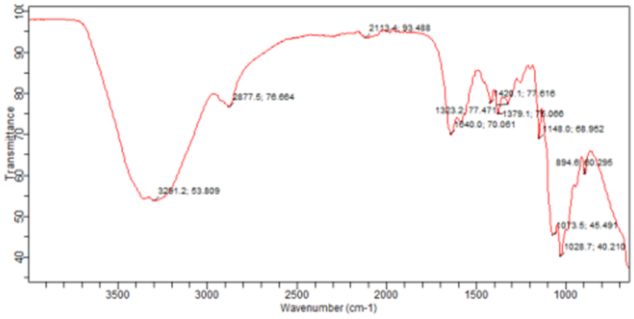

Figure 4: FT-IR spectrum of chitosan.

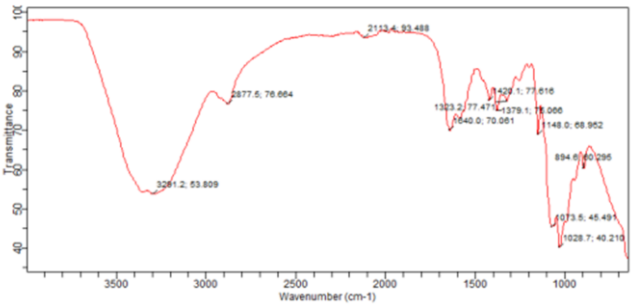

Figure 5: FT-IR spectrum of calcium chloride.

SCVJ
Volume 4, Issue 2, 2023
DOI: http://doi.org/10.55989/KLYA6292
Science View Journal
ISSN (Online): 2734-2638

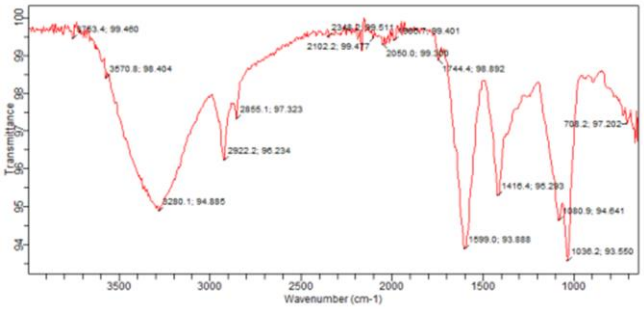

Figure 6: FT-IR spectrum of yellow fever vaccine

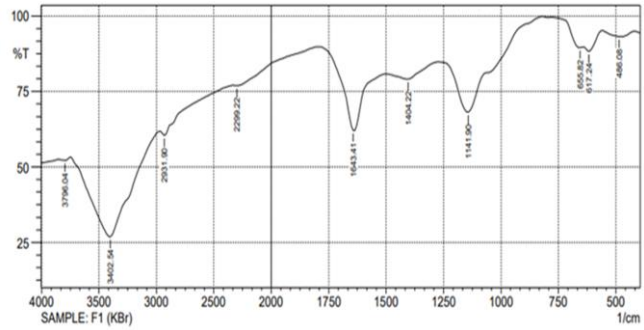

Figure 7: FT-IR spectrum of the PRSYFV vaccine.

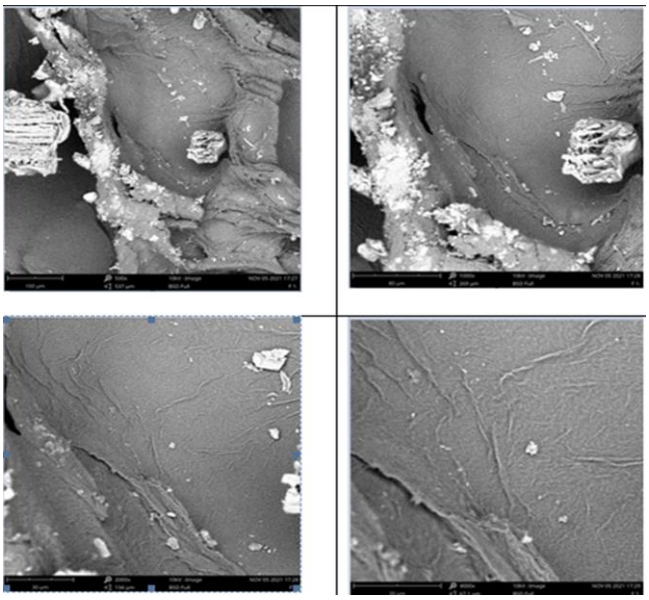

Figure 8: Photomicrograph of the PRSYFV vaccine surface

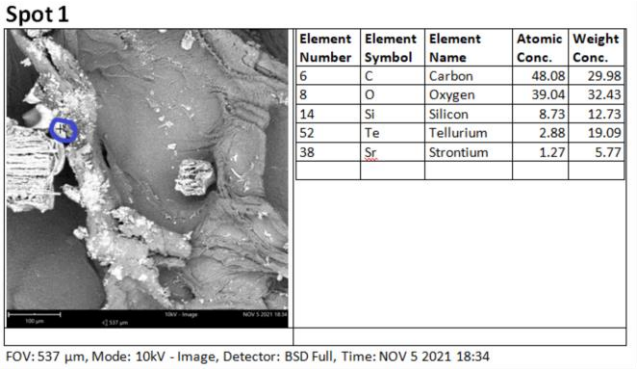

Element Number	Element Symbol	Element Name	Atomic Conc.	Weight Conc.
6	C	Carbon	48.08	29.98
8	O	Oxygen	39.04	32.43
14	Si	Silicon	8.73	12.73
52	Te	Tellurium	2.88	19.09
38	Sr	Strontium	1.27	5.77

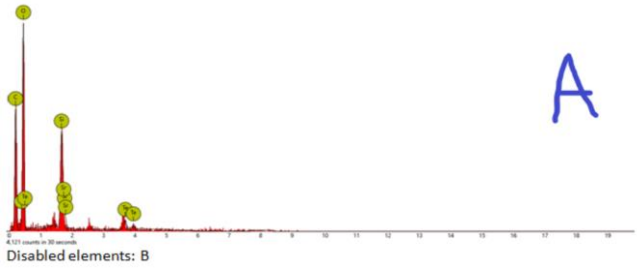

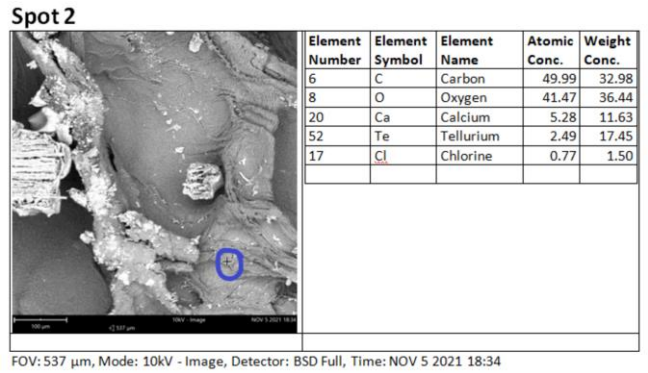

Element Number	Element Symbol	Element Name	Atomic Conc.	Weight Conc.
6	C	Carbon	49.99	32.98
8	O	Oxygen	41.47	36.44
20	Ca	Calcium	5.28	11.63
52	Te	Tellurium	2.49	17.45
17	Cl	Chlorine	0.77	1.50

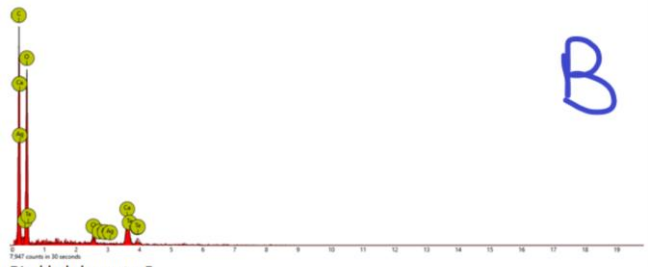

Figure 9: Energy-dispersive X-ray spectra of PRSYFV vaccine surface.

Note: Spot 1 shows the crystal deposition and spot 2, the surface composition with subsequent analysis (A and B). Notice the silicon atoms in the crystal and the surface is mostly composed of oxygen and calcium.

IV. Discussion

The FTIR technique has been extensively used to kindle vibrational levels of known chemical groups in a molecule so as to identify them. FTIR spectral analysis of the individual ingredients and final PRSYFV vaccine obtained was essential to confirm the chemical compatibility of all the constituents on microcapsule formation, evidenced by changes in

SCVJ
Volume 4, Issue 2, 2023
DOI: http://doi.org/10.55989/KLYA6292
Science View Journal
ISSN (Online): 2734-2638

characteristics spectral peaks. FT-IR spectrum of the RHA SiO2 NPs showed four (4) characteristic peaks at 3365.8, 1636.3, 1051.1 and 793.9 cm-1 wavelength as shown in Figure 2. The peak at 3365.8 cm-1 wavelength is assigned to the O-H stretching vibrations of carboxylic acid (FTIR correlation table) while the peak at 1636.3cm-1 wavelength is equivalent to aromatic C=C stretching vibration and/or asymmetric C=O stretching vibration (Kora et al., 2012; Litvin and Minaev, 2013; Lazar et al., 2012). The intense peak at 1051.1 cm-1 wavelength may be given to C–O stretching (Litvin and Minaev 2013; Gajbhiye et al., 2009; Lazar et al., 2012) and the peak at 793.9 cm-1 wavelength could be assigned to the C-Cl bond seen in chloroalkane (Lazar et al., 2012). FT-IR spectrum for sodium alginate shows various characteristic peaks as shown in Figure 3. Distinctive FT-IR bands of sodium alginate are consistent with published data (Sankalia et al., 2007). Key absorption bands for the hydroxyl, carboxylic and ether functional groups are shown. Stretching vibrations of O–H bonds of alginate occurred at 3242.8cm-1 wavelength. Stretching vibrations of aliphatic C–H appeared in 2926cm-1 wavelength. Observed bands in 1405.2 and 1591.6 cm-1 wavelength were ascribed to symmetric and asymmetric stretching vibrations of carboxylate salt ion, respectively. The peaks at 1297.1 and 946.7 cm-1 wavelength were assigned to the C–O stretching vibration of pyranosyl ring and the C–O stretching with contributions from C–C–H and C–O–H deformation (Daemi et al., 2012). Figure 4 depicts the FT-IR spectrum of chitosan, which displayed a number of distinctive peaks. In this spectrum, the wide absorption band at 3291.2cm-1 wavelength is attributed to the O-H stretching vibrations of water and hydroxyl overlapped with N-H stretching vibrations of free amino groups, 2877.5cm-1 for aliphatic C-H stretching vibrations of CH3 and CH2 in the chitosan (Guo et al., 2005). The peak at 1323.2cm-1 is ascribed to the C-O stretching vibration of key alcoholic groups and 1073.5cm-1 for the stretching vibration of hydroxyl group of C3-OH (Monvisade and Siriphannon 2009; Zhang et al., 2011).The sharp peak at 1640.0cm-1 is attributed to the in-plane N-H bending vibration of NH2 which is a distinguishing peak of chitosan polysaccharide and also a marker for the presence of deacetylation (Zhang et al. 2011; Mohanasrinivasan et al., 2014). And the peak at 1028.7cm–1 may perhaps correspond to the stretching of C6 -OH hydroxyl groups. The peak at 894.6cm–1 is tied to the distinctive skeletal vibration of β-anomers (Zhang et al. 2011). Similar peaks were found by Paulino et al., 2009 and Reinas et al., 2014 when they analyzed the infrared spectrum of chitosan. The calcium chloride FT-IR spectrum had 11 distinguishing peaks as illustrated in Figure 5. These characteristic peaks were seen at 3783.2, 3652.8, 3481.3, 3369.5, 2344.5, 2109.7, 1982.9, 1800.3, 1621.4, 1300.8 and 842.4cm-1 wavelength. The stretching vibrations at 3783.2, 3652.8, 3481.3 and 3369.5cm-1 wavelength relate to asymmetric –OH stretch, while the peaks at 2344.5, 2109.7 and 1982.9cm-1 wavelength peaks correspond to symmetric O–H stretch; 1800.3cm-1 wavelength peak is attributed to the aromatic C=C stretching vibration and/or asymmetric C=O stretching vibration (Kora et al. 2012; Litvin and Minaev, 2013; Lazar et al., 2012). The 1621.4cm-1 wavelength peak is assigned to H–O–H bending vibration bands owing to the water in CaCl2 (Araujo et al., 2021). The appearance of several peaks instead of the usual single peak for asymmetric O–H stretching and H–O–H bending is suggestive of various hydrogen bonding conditions brought on by interactions with chloride ions and water molecules (Karunadasa, 2019). The band at 1300.8 cm-1 wavelength could be associated with C-O stretching vibration of principal alcoholic groups. The band at 842.4 cm-1 wavelength could be attributed to Ca–O stretching characteristic of calcium chloride (Cho et al., 2014). The FT-IR spectra of calcium chloride, chitosan and sodium alginate obtained are in agreement with what is published in literature, revealing similar peaks (Guo et al., 2005; Monvisade and Siriphannon 2009; Zhang et al. 2011; Mohanasrinivasan et al., 2014; Kora et al. 2012; Litvin and Minaev, 2013; Cho et al. 2014; Daemi et al., 2012, Sankalia et al. 2007). These shows the powders were pure and uncontaminated. The FT-IR spectrum of the yellow fever vaccine showed 15 peaks as depicted in Figure 6. These peaks were seen at 3753.4, 3570.8, 3280.1, 2922.2, 2855.1, 2348.2, 2102.2, 2050.0, 1986.7, 1744.4, 1599.0, 1416.4, 1080.9, 1036.2 and 708.2cm-1 wavelength. The stretching vibrations at 3753.4, 3570.8 and 3280.1 cm-1 wavelength are attributed to the vibration of hydroxyl (–OH) functional group. The peaks at 2922.2 and 2855.1cm-1 wavelength correspond to C-H stretching vibration. While the peaks at 2348.2, 2102.2, 2050.0 and 1986.7cm-1 wavelength correspond to symmetric O–H stretch (Araujo et al., 2021). Peaks at 1744.4 and 1599.0 cm-1 wavelength relates to aromatic C=C stretching vibration and/or asymmetric C=O stretching vibration and/or C=N stretching vibration (Kora et al. 2012; Litvin and Minaev, 2013; Lazar et al., 2012). The peaks at 1416.4, 1080.9 and 1036.2cm-1 wavelength could be attributed to C-O and/or C-C stretching vibration while the peak at 708.2cm-1 wavelength could be assigned to C-Cl vibration. The yellow fever vaccine has so many peaks as expected as it is made up of different ingredient (YF-17D virus, excipents, etc). FT-IR spectrum of the PRSYFV vaccine revealed 10 peaks as shown in Figure 7. These peaks were seen occurring at 3796.04, 3402.54, 2931.90, 2299.22, 1643.41, 1404.22, 1141.90, 655.82, 617.24 and 486.06. The peaks at 3796.04 and 3402.54 cm-1 wavelengths are ascribed to the hydroxyl (-OH) stretching vibrations. Peaks at 2931.90 and 2299.22cm-1 wavelength corresponds to the C-H stretching vibration of aliphatic group. The peak at 1643.41cm-1 wavelength relates to aromatic C=C stretching vibration and/or asymmetric C=O stretching vibration (Kora et al. 2012; Litvin and Minaev, 2013; Lazar et al., 2012). The peaks after 1500cm-1 wavelength which constitute the fingerprint regions are often difficult to interpret. The peaks at 1404.22 and 1141.90cm-1 wavelength could be attributed to C-O and/or C-C stretching vibration while the peak at 655.82 and 617.24cm-1 wavelength could be ascribed to C-Cl vibration. The peak at 486 cm-1 wavelength may be assigned to C-l vibration (Lazar et al., 2012). The FTIR spectra of the PRSYFV vaccine which contains sodium alginate, YFV, calcium chloride, chitosan and RHA SiO2 NPs mixture shows peaks representative of these ingredients with a little interference or changes in the bond peak activity. The –OH stretching vibration band present in the individual ingredients was seen occurring at 3402 cm–1. The 2926.0 peak for C-H stretching vibration in sodium alginate was

SCVJ
Volume 4, Issue 2, 2023
DOI: http://doi.org/10.55989/KLYA6292
Science View Journal
ISSN (Online): 2734-2638

shifted to 2931.90 in the PRSYFV vaccine. The N-H bending vibration at 1640cm-1 indicative of chitosan was still retained but moved to 1643cm-1 after complexation with alginate showing the amino group of chitosan and carbonyl group of sodium alginate had an ionic interaction. Formation of capsules made of sodium alginate and chitosan is as a result of strong interactions through hydrogen bonds between the functional groups of the two polymers in which chitosan's amino and amide groups participate, as a result, the absorption bands of the amino and amide groups changed in the FT-IR spectra. The 1148.0 C-O peak in chitosan was moved to 1141.90 in the mixture and it is more intense in the mixture. The 1416.4 and 1420.1 cm-1 wavelength C-O stretching vibration in YFV and chitosan respectively was equally moved to 1404.22 in the mixture and the intensity was reduced. This implies that the interactions that formed the microgel might have involved carboxylate and possibly even hydroxyl groups. The slight changes of characteristics spectral bands are indicative of the chemical reaction of the formulation ingredients.

Scanning electron microscopy (SEM) has been used in assessing prospective wall/coating materials for any specific microencapsulation procedure. By integrating the unique information offered by SEM with other chemical investigations, microcapsules of high quality could be chosen successfully since their physical properties and functionality are closely tied to their microstructure (Santiworakun et al., 2022). The scanning electron microscopy uses a highly active and focused electron beam to scan the sample and often produces an immensely magnified image of the sample's morphology, while details on its chemical makeup are provided by the energy dispersive X-ray spectrometer (EDX) detector. EDX spectra directly reveals the presence of the atomic elements in the sample; hence, EDX analysis was performed in order to confirm the formation of the PRSYFV vaccine with the ingredients used. SEM studies of the PRSYFV vaccine at different magnifications (500X, 1000X, 2000X and 4000X) revealed the PRSYFV vaccine had uneven and rough surfaces with shrinkages. This finding is in line with the research of Islam et al., 2011. The wrinkled surface is a feature of the alginate polymer used (Pasparakis and Bouropoulos, 2006) and is likely due to the evaporation of water originally trapped within the hydrogel matrix (Yeung et al., 2016). Interestingly, the uneven microcapsule surfaces had different tiny crystal depositions at various locations across the surface, either as big or small clumps. Examination of the crystal deposits on the microcapsule surfaces (Figure 9) showed the presence of silicon atoms, confirming that the tiny crystals seen on the microcapsules's surface were that of silica nanoparticles (as no other component of the formulation contains silicon). The SEM-EDX analyses showed the RHA silica nanoparticles coated the microcapsule surface, and was not washed off during the washing step showing a good network/interaction with the polymer. The spectra of chemical analysis revealed the predominant atoms were C, O, Ca, Si, Na and Cl as expected for a typical microcapsule made by ionic-gelation technique (Awasthi and Kulkarni, 2012). The microcapsule surface composition showed the surface is mainly composed of calcium and oxygen, which is as expected for microcapsules created via the ionic gelation process, as the surface composition is primarily calcium alginate (Awasthi and Kulkarni, 2012). The silicon atom was exclusive to the crystal deposition, which demonstrated preferential binding to the microcapsule surface; Na and Cl represents sodium chloride, which is the by-product of ionic gelation of Ca with O, and was expected, given that the microcapsule surface is mainly made of calcium alginate (Awasthi and Kulkarni, 2012; Mooranian et al., 2014). The encapsulation of the yellow fever virus vaccine into the polymer-silica blend was efficient as seen from the vaccine encapsulation efficiency of 66.7%, it shows the vaccine was entrapped within the polymer-silica blend. Efficiency of encapsulation is an important parameter used to indicate the capability of a carrier matrix to encapsulate the vaccine antigen.

V. Conclusion

Overall, FTIR spectra of the ingredients and final PRSYFV vaccine and the SEM-EDX of the PRSYFV vaccine suggest good chemical compatibility of all the ingredients in the PRSYFV formulation. It also shows the microencapsulation of yellow fever vaccine within polymer-silica blend does not appreciably alter the chemical make-up or structural integrity of the molecules that make up the yellow fever vaccine, since there was no substantial chemical interaction between the vaccine antigen and any of the formulation ingredients. The polymer-silica matrix demonstrated good encapsulating ability with an above average vaccine encapsulation efficiency. Since there were no appreciable changes in the chemical composition of the components on microencapsulation, it seems reasonable to draw the conclusion that no chemical reactions or decomposition took place before and after microencapsulation, other than what was necessary to create the PRSYFV vaccine.

VI. References

Alhadhrami, A., Mohamed, G. G., Sadek, A. H., Ismail, S. H., Ebnalwaled, A. A., & Almalki, A. S. A. (2022). Behavior of Silica Nanoparticles Synthesized from Rice Husk Ash by the Sol-Gel Method as a Photocatalytic and Antibacterial Agent. Materials (Basel, Switzerland), 15(22), 8211.

Araujo, J. A., Cortese, Y. J., Mojicevic, M., Brennan Fournet, M., & Chen, Y. (2021). Composite Films of Thermoplastic Starch and CaCl2 Extracted from Eggshells for Extending Food Shelf-Life. Polysaccharides, 2, 677–690.

Awasthi, R., & T Kulkarni, G. (2012). Development of novel gastroretentive floating particulate drug delivery system of gliclazide. Current drug delivery, 9, 437–451.

Bankole, A. M., Olusegun, K.-K., Marian, N. B., Godswill, I., Adebowale, O. A., Lukeman, A. S., et al. (2010). The impact of health facility monitoring on cold chain management practices in Lagos, Nigeria. Journal of Public Health and Epidemiology, 2, 78–81.

DOI: http://doi.org/10.55989/KLYA6292

Bassey, B. E., Braka, F., Onyibe, R., Kolude, O. O., Oluwadare, M., Oluwabukola, A., et al. (2022). Changing epidemiology of yellow fever virus in Oyo State, Nigeria. BMC Public Health, 22, 1–7.

Cho, A. R., Chun, Y. G., Kim, B. K., & Park, D. J. (2014). Preparation of alginate–CaCl 2 microspheres as resveratrol carriers. Journal of Materials Science, 49, 4612–4619.

Daemi, H.,&Barikani, M. (2012).Synthesis and characterization of calcium alginate nanoparticles, sodium homopolymannuronate salt and its calcium nanoparticles.ScientiaIranica F 19:2023-2028.

Epstein, E. (2001). Silicon in plants: facts vs. concepts, in L. E. Dantoff, G. H. Snyder, G.H. Korndoper (Eds.): Silicon in agriculture. Elsevier Science, Amsterdam, pp. 1 – 15.

Gajbhiye, M., Kesharwani, J., Ingle, A., Gade, A., & Rai, M. (2009). Fungus-mediated synthesis of silver nanoparticles and their activity against pathogenic fungi in combination with fluconazole. Nanomedicine: Nanotechnology, Biology and Medicine, 5, 382–386.

Grimes, S. E. (2002). A basic laboratory manuel for the small scale production and testing of 1-2 Newcastle disease vaccine. Food and Agricultural organisation-Regional office for Asia and the Pacific (FAO-RAP) publication 2002/22.ISBN 974-7946-26-2.

Guo, Z., Xing, R., Liu, S., Yu, H., Wang, P., Li, C., & Li, P. (2005). The synthesis and antioxidant activity of the Schiff bases of chitosan and carboxymethyl chitosan. Bioorganic & medicinal chemistry letters, 15(20), 4600-4603.

Hung, D.P., Vuong, N.T., Hieu, D.M., Linh, N.T., Thanh, T.V., Phuc, M.V., Hiep, N.A., Tien, D.M. (2018). Effect of silica nanoparticles on properties of coatings based on acrylic emulsion resin. Vietnam Journal of Science and Technology, 56 (3B), 117-125.

Islam, M. M., Masum, S. M., Rahman, M. M., Molla, M. A., Shaikh, A. A., & Roy, S. K. (2011). Preparation of chitosan from shrimp shell and investigation of its properties. International Journal of Basic & Applied Sciences, 11, 77–80.

Karunadasa, S. (2019). Dehydration of Calcium Chloride as Examined by High-temperature X-ray Powder Diffraction. Int. Multidiscip. Res. J, 4, 37–43.

Kora, A. J., Sashidhar, R. B., & Arunachalam, J. (2012). Aqueous extract of gum olibanum (Boswellia serrata): a reductant and stabilizer for the biosynthesis of antibacterial silver nanoparticles. Process Biochemistry, 47, 1516–1520.

Kumari, A., Yadav, S. K., Yadav, S. C. (2010). Biodegradable polymeric nanoparticles based drug delivery systems. Colloids and Surfaces. B, Biointerfaces, 75(1), 1-18.

Lazar, G., Ureche, D., Ifrim, I. L., Stamate, M., Ureche, C., Nedeff, V., Nistor, I. D., Finaru, A. L. & Lazar, I. M. (2012). Effects of the environmental stress on two fish populations revealed by statistical and spectral analysis. Environmental Engineering and Management Journal, 11(1), 109-124.

Litvin, V. A., & Minaev, B. F. (2013). Spectroscopy study of silver nanoparticles fabrication using synthetic humic substances and their antimicrobial activity. Spectrochimica Acta Part A: Molecular and Biomolecular Spectroscopy, 108, 115–122.

Luria-Pérez, R., Sánchez-Vargas, L. A., Muñoz-López, P., & Mellado-Sánchez, G. (2022). Mucosal Vaccination: A Promising Alternative Against Flaviviruses. Frontiers in Cellular and Infection Microbiology , 726.

Mohanasrinivasan, V., Mishra, M., Paliwal, J. S., Singh, S. K., Selvarajan, E., Suganthi, V., et al. (2014). Studies on heavy metal removal efficiency and antibacterial activity of chitosan prepared from shrimp shell waste. 3 Biotech, 4, 167–175.

Monvisade, P., & Siriphannon, P. (2009). Chitosan intercalated montmorillonite: Preparation, characterization and cationic dye adsorption. Applied Clay Science, 42, 427–431.

Mooranian, A., Negrulj, R., Chen-Tan, N., Al-Sallami, H. S., Fang, Z., Mukkur, T. K., et al. (2014). Microencapsulation as a novel delivery method for the potential antidiabetic drug, Probucol. Drug design, development and therapy , 1221–1230.

Oli, A. N., Agu, R. U., Ihekwereme, C. P., & Esimone, C. O. (2017). An evaluation of the cold chain technology in South-East, Nigeria using immunogenicity study on the measles vaccines. The Pan African Medical Journal, 27.

Pasparakis, G., & Bouropoulos, N. (2006). Swelling studies and in vitro release of verapamil from calcium alginate and calcium alginate–chitosan beads. International journal of pharmaceutics, 323, 34–42.

Paulino, A. T., Guilherme, M. R., de Almeida, E. A., Pereira, A. G., Muniz, E. C., & Tambourgi, E. B. (2009). One-pot synthesis of a chitosan-based hydrogel as a potential device for magnetic biomaterial. Journal of Magnetism and Magnetic Materials, 321, 2636–2642.

Rains, D. W., Epstein, E., Zasoski, R. J., & Aslam, M. (2006). Active silicon uptake by wheat. Plant and Soil, 280, 223–228.

DOI: http://doi.org/10.55989/KLYA6292

Ray, S. S. & Okamoto, M. (2003). Polymer/layered silicate nanocomposites: A review from preparation to processing. Progress in Polymer Science, 28, 1539–1641.

Reinas, A. E., Hoscheid, J., Outuki, P. M., & Cardoso, M. L. (2014). Preparation and characterization of microcapsules of Pterodon pubescens Benth. by using natural polymers. Brazilian Journal of Pharmaceutical Sciences, 50, 919–930.

Ribeiro, T., Baleizão, C. & Farinha, J. P. S. (2014). Functional Films from Silica/Polymer Nanoparticles. Materials, 7, 3881-3900.

Sankalia, M. G., Mashru, R. C., Sankalia, J. M., & Sutariya, V. B. (2007). Reversed chitosan–alginate polyelectrolyte complex for stability improvement of alpha-amylase: Optimization and physicochemical characterization. European journal of pharmaceutics and biopharmaceutics, 65, 215–232.

Sankar, S., Sharma, S. K., Kaur, N., Lee, B., Kim, D. Y., Lee, S., et al. (2016). Biogenerated silica nanoparticles synthesized from sticky, red, and brown rice husk ashes by a chemical method. Ceramics International, 42, 4875–4885.

Santiworakun, N. Y., Suksuwan, A., Sirikwanpong, S., Dahlan, W., & Ariyapitipun, T. (2022). Physicochemical characterization of microcapsules containing cold pressed black cumin seed oils (Nigella sativa L.) as an alternative nutrient source in a functional diet. LWT, 157, 113045.

Shang, X.-Y., Zhu, Z.-K., Yin, J. & Ma, X.-D. (2002). Compatibility of soluble polyimide/silica hybrids induced by a coupling agent. Chem. Mater., 14, 71–77.

Witoon, T., Chareonpanich, M., Limtrakul, J. (2008). Synthesis of bimodal porous silica from rice husk ash via sol–gel process using chitosan as template. Materials Letters, 62 (10–11), 1476-1479.

Yeung, T.W., Ucok, E.F., Tiani, K.A. McClements, D.J and Sela, D.A. (2016).Microencapsulation in alginate and chitosan microgels to enhance viability of Bifidobacteriumlongum for oral delivery.Frontiers in Microbiology, 7, 494.

Zhang, A. J., Qin, Q.-L., Zhang, H., Wang, H.-T., Li, X., Miao, L., et al. (2011). Preparation and characterisation of food grade chitosan from housefly larvae. Czech Journal of Food Sciences, 29, 616–623.

Zhang, S., Yu, A., Song, X. & Liu, X. (2013). Synthesis and characterization of waterborne UV-curable polyurethane nanocomposites based on the macromonomer surface modification of colloidal silica. Prog. Org. Coat., 76, 1032–1039.

Zhou, Y., Martins, E., Groboillot, A., Champagne, C., and Neufeld, R. (1998).Spectrophotometric quantification of lactic bacteria in alginate and control of cell release with chitosan coating. J. Appl. Microbiol. 84, 342–348.